ACS OMEGA

Article

Cite This: ACS Omega 2018, 3, 9598−9606

http://pubs.acs.org/journal/acsodf

Nanostructured Silicon−Carbon 3D Electrode Architectures for High-Performance Lithium-Ion Batteries

Sarode Krishna Kumar,[†] Sourav Ghosh,[†] Sairam K. Malladi,[‡] Jagjit Nanda,[§] and Surendra K. Martha*[,†]

[†]Department of Chemistry and [‡]Department of Materials Science and Metallurgical Engineering, Indian Institute of Technology Hyderabad, Kandi, Sangareddy 502285, Telangana, India

[§]Materials Science and Technology Division, Oak Ridge National Laboratory, Oak Ridge, 37831, Tennessee, United States

Supporting Information

ABSTRACT: Silicon is an attractive anode material for lithium-ion batteries. However, silicon anodes have the issue of volume change, which causes pulverization and subsequently rapid capacity fade. Herein, we report organic binder and conducting diluent-free silicon−carbon 3D electrodes as anodes for lithium-ion batteries, where we replace the conventional copper (Cu) foil current collector with highly conductive carbon fibers (CFs) of 5−10 μm in diameter. We demonstrate here the petroleum pitch (P-pitch) which adequately coat between the CFs and Si-nanoparticles (NPs) between 700 and 1000 °C under argon atmosphere and forms uniform continuous layer of 6−14 nm thick coating along the exterior surfaces of Si-NPs and 3D CFs. The electrodes fabricate at 1000 °C deliver capacities in excess of 2000 mA h g^{-1} at C/10 and about 1000 mA h g^{-1} at 5 C rate for 250 cycles in half-cell configuration. Synergistic effect of carbon coating and 3D CF electrode architecture at 1000 °C improve the efficiency of the Si−C composite during long cycling. Full cells using Si−carbon composite electrode and $Li_{1.2}Ni_{0.15}Mn_{0.55}Co_{0.1}O_2$-based cathode show high open-circuit voltage of >4 V and energy density of >500 W h kg^{-1}. Replacement of organic binder and copper current collector by high-temperature binder P-pitch and CFs further enhances energy density per unit area of the electrode. It is believed that the study will open a new realm of possibility for the development of Li-ion cell having almost double the energy density of currently available Li-ion batteries that is suitable for electric vehicles.

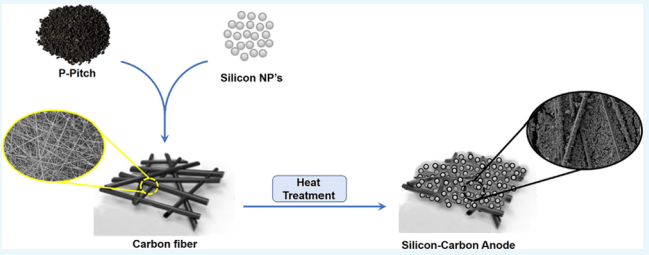

1. INTRODUCTION

US Department of Energy (DOE) and the United States Advanced Battery Consortium LLC (USABC)'s 2020 roadmap or the next-generation lithium-ion batteries target electric vehicle pack energy density of 275 W h kg^{-1} or 550 W h L^{-1} at a cost of $125/kW h or below.[1] This, if achieved, would enable a large market penetration of pure electric-driven vehicles. Besides, the lithium-ion batteries should have improved safety and cycle life. Therefore, current research emphasis is given to develop high energy-density cathodes and high voltage electrolytes coupled with high capacity silicon anodes for increasing the energy density in Li-ion batteries.[2−8] Current state-of-the-art lithium-ion cells use layered transition metal (TM) oxide cathodes (e.g., $LiCoO_2$, $LiNi_{0.8}Co_{0.15}Al_{0.15}O_2$, and $LiNi_{1/3}Mn_{1/3}Co_{1/3}O_2$), or phosphates (e.g., $LiFePO_4$), Mn-based spinels ($LiMn_2O_4$, $LiMn_{1.5}Ni_{0.5}O_4$), and graphitic carbons as anodes.[2] The useable capacity of most of these cathode systems is in the range between 140 and 180 mA h g^{-1} when cycled up to 4.2 V, whereas the most commercially used anode, graphite, is around 350 mA h g^{-1}.[2] Thus, there has been an intense research activity during the last couple of decades to develop high capacity or high energy cathodes and anodes for lithium-ion batteries. Li−Mn-rich (LMR)-based compounds, such as $Li_{1.2}Mn_{0.55}Ni_{0.15}Co_{0.1}O_2$, lithium, and manganese-rich TM oxide (LMR−NMC) composite cathodes, promise almost double the capacity (372 mA h g^{-1} for 1.2 Li transfer) of currently available cathodes that have been investigated as a promising cathode material for lithium-ion batteries.[3−6] To enhance the performance of anodes which meet the requirement of the automotive industry, researchers have been investigating materials which form alloys with lithium to generate anodes that have specific capacities on the order of magnitude higher than graphite.[7,8] Silicon is an attractive anode material for Li-ion batteries mainly because of its very high theoretical charge capacity of 4200 mA h g^{-1} ($Li_{4.4}Si$) and natural abundance.[7−14] However, despite such potential, silicon has a number of fundamental materials challenges that has impeded its growth toward commercialization. First, it undergoes tremendous volume changes under lithiation (and delithiation), which can be as high as 310% for the maximum lithiated phase of $Li_{3.75}Si$ (at room temperature).[7−14] This phenomenon leads to constant formation and reformation at

Received: May 7, 2018
Accepted: August 7, 2018
Published: August 21, 2018

DOI: 10.1021/acsomega.8b00924
ACS Omega 2018, 3, 9598−9606

the interface creating new solid electrolyte interphase (SEI) layer during each cycle amounting to loss of lithium inventory to capacity fade. Further, Si surface has inevitably a native oxide layer and has different surface reactivity and passivation (with respect to the electrolyte) that significantly affect the electrochemical reversibility.[7−14] These combined challenges make pure silicon anodes almost impractical for any near-term application unless the fundamental issues are addressed.[10−12] There has been an intense research to mitigate volume change during cycling, such as producing Si-nanoparticles (NPs),[7,10,13−15] aligned Si-nanowires/nanotubes,[9,16−19] dispersing silicon into an active (such as carbon)/inactive (e.g., SiO_2) matrix,[20−29] silicon-based thin films,[30−34] free standing Si−C electrodes, and different morphologies of silicon.[35−41] Taking benefit of high conductivity of carbon and high-capacity silicon, recent reports demonstrate that carbon−silicon nanocomposites can circumvent the issues associated with silicon and improve the overall electrochemical performance of Si-anode for Li-ion batteries.[20−34] This is because silicon−carbon nanocomposites can accommodate a huge strain with reduced pulverization, provide good electronic contact, and exhibit short diffusion path for lithium-ion insertion.

Another interesting approach of silicon−carbon composite free-standing electrodes (binder less and current collector less) which are flexible is used to create thin and flexible lithium-ion batteries.[35−41] Self-standing anodes consisting of molecular precursor-derived silicon oxycarbide glass particles embedded in a chemically modified reduced graphene oxide matrix show reversible capacities of ∼702 mA h g^{-1} at the 1st cycle and ∼588 mA h g^{-1} at the 1020th cycle, respectively without any mechanical failure.[35] Composites of Si-NPs and graphene accommodated on a three-dimensional (3D) network of graphite exhibited high Li-ion storage capacities of >2200 mA h g^{-1} after 50 cycles and >1500 mA h g^{-1} after 200 cycles.[36] Freestanding macroporous silicon film in combination with pyrolyzed polyacrylonitrile composite anode shows a discharge capacity of 1260 mA h g^{-1} for 20 cycles.[37] Lightweight free-standing carbon nanotube−silicon films prepared by sputtering method shows a specific charge-storage capacity (∼2000 mA h g^{-1}) for 50 cycles.[38] Binder and additive-free 3D porous nickel-based current collector coated conformally with layers of silicon delivers high capacity of 1650 mA h g^{-1} after 120 cycles of charge−discharge.[39] Overall, silicon−carbon composite free-standing electrodes prepared by various synthesis approaches show a capacity between 700 and 2200 mA h g^{-1} for about 100−500 cycles. Free-standing electrodes have an overall limited cell capacity because of low loading of active masses (1−2 mg cm^{-2}, submicron thickness); expensive techniques are employed for synthesis; and most importantly, free-standing paper electrodes show high irreversible capacity loss (∼50%), low cycling efficiency (95−98%), and poor capacity retention at high current densities and so forth.

Here, we present a unique organic binder-less, additive free 3D electrode architecture of silicon−carbon NPs on carbon fiber (CF) current collector which replaces usual copper foil current collector.[42,43] Petroleum pitch (P-pitch) is used as a carbon source which makes a good electrical contact between the CF current collector and Si-active particles at high temperatures >500 °C. CF mat has numerous advantages over copper current collector such as incorporation of large amount of active material into the 3D CF network and provides high interfacial contact of active material to the conductive network. Besides, the CFs are more flexible, having good mechanical strength and can accommodate the volume change of silicon. However, the silicon NPs will lose the contact from CF because of the absence of binder. Therefore, there is need of a material which supports the volume change, improves conductivity, and binds silicon on to CF. Petroleum pitch which is a complex mixture of polynuclear aromatic hydrocarbons, derived from heat treatment of coal and petroleum tars, can be used as a high-temperature binder to bind Si-NPs on to CF. Pitch undergoes carbonization above 500 °C to form a conducting carbon through mesophase (liquid crystalline state).[44] Therefore, annealing mixture of P-pitch and silicon NPs coated on to CF current collector at high temperatures ≥500 °C melts the P-pitch and allows the conformal coating throughout the silicon and CF which enables to have a conductive network and enough space for the volume expansion and contraction without undergoing pulverization. In addition, the binding strength of carbonized pitch with silicon and CF is influenced by temperature. In this work, we have studied the effect of different annealing temperatures (700, 900, and 1000 °C) on the electrochemical performance of silicon−carbon 3D electrodes. Electrodes developed by this method provide enough space for silicon surrounded by carbonized pitch on CFs which support the volume expansion and contraction during cycling, thus reducing the pulverization of the silicon. In this type of electrode, all of the active material is exposed to electrolyte which implies that the entire silicon is electrochemically active, whereas in conventional composite electrode in which copper foil is used as current collector, interior part of the electrode is electrochemically inactive because of lack of access to electrolyte. Moreover, polyvinylidene fluoride (PVdF) binder in the composite electrode causes impedance rise, leading to detrimental in the electrochemical performance. In addition, copper foil adds extra weight to the electrode. However, 3D Si−C free-standing CF electrodes do not contain any organic binder and less weight. Besides, carbonized pitch delivers capacity of about 10% to the total capacity of the electrode. This would further enhance energy density. The electrode fabrication process is similar to a solid-state method, which is inexpensive and scalable.

2. RESULTS

The diffraction patterns of Si-NPs are shown in Figure 1. The diffraction planes (111), (220), and (311) at Bragg positions of 28.66°, 47.57°, and 56.39° correspond to pure silicon (face-centered cubic lattice, space group: *Fd*3*m*, JCPDS no. 895012). X-ray diffraction (XRD) of Si−C composite electrodes fabricated at different temperatures shows the corresponding peaks of carbon and silicon suggesting the successful blend of Si−C composite. The weak and broad peak between 20° and 30° of (002) plane indicates the formation of amorphous carbon. As annealing temperature increases, there is an increase in the intensity of carbon peak, which indicates the increase in crystallinity. The *d*-spacing values of broad peak in Si−C composite formed by annealing at 700, 900, and 1000 °C are 3.65, 3.57, and 3.52 Å, respectively. The decrease in *d*-spacing value with increase in temperature clearly indicates the increase of ordering of carbon.[45]

Si-NPs synthesized by magnesiothermic reduction are of typical spherical morphology having particle sizes in the range of 50−100 nm (Figure 2a). Three-dimensional Si−C composite free-standing electrodes fabricated at temperatures

DOI: 10.1021/acsomega.8b00924
ACS Omega 2018, 3, 9598−9606

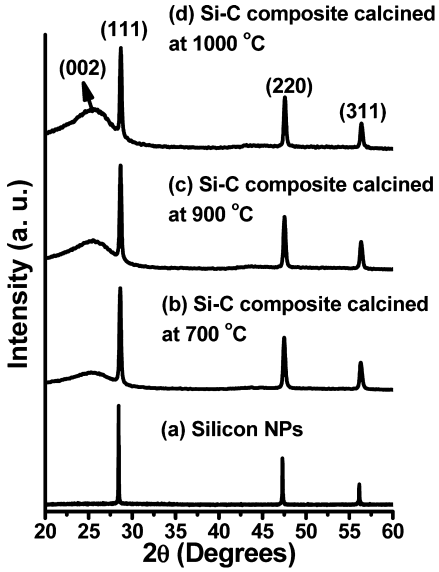

Figure 1. XRD patterns of the as-synthesized (a) silicon NPs and 3D Si−C free-standing composite electrodes annealed at (b) 700, (c) 900, and (d) 1000 °C.

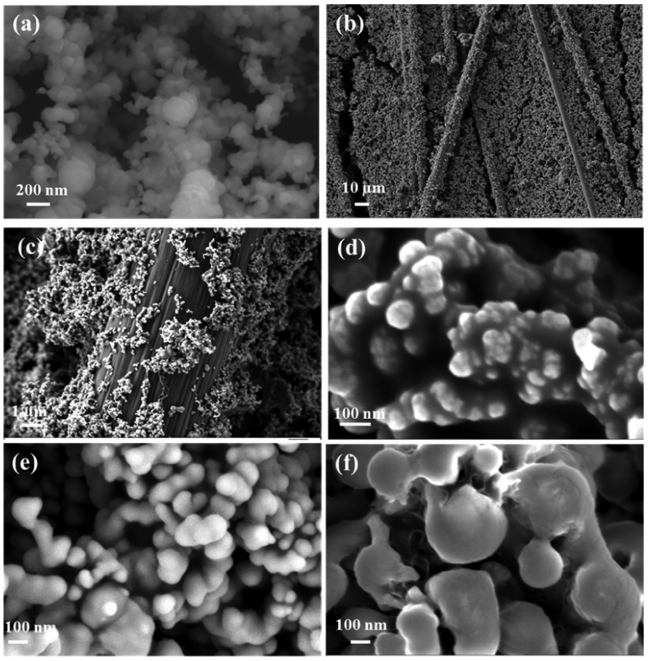

Figure 2. Field-emission scanning electron microscopy (SEM) images of (a) silicon NPs synthesized by magnesiothermic reduction; (b) Three-dimensional Si−C composite electrode; (c) high-resolution image 3D Si−C composite electrode; silicon−carbon composite annealed at (d) 700, (e) 900, and (f) 1000 °C.

of 700, 900, and 1000 °C are shown in Figure 2b,c. At high temperatures >700 °C, P-pitch coats on to the fiber and Si-NPs and makes a good electronic contact along and between the fibers and on to the particle. Typically, pitch forms about 6−14 nm of C coating onto Si-NPs when annealed at the temperatures between 700 and 1000 °C (discussed later in Figure 3). The 3D electrode architecture of Si-NPs on CF electrode shows a uniform distribution of silicon and carbon throughout the CF. The high-resolution image (Figure 2c) indicates the good binding of Si−C composite on CF with

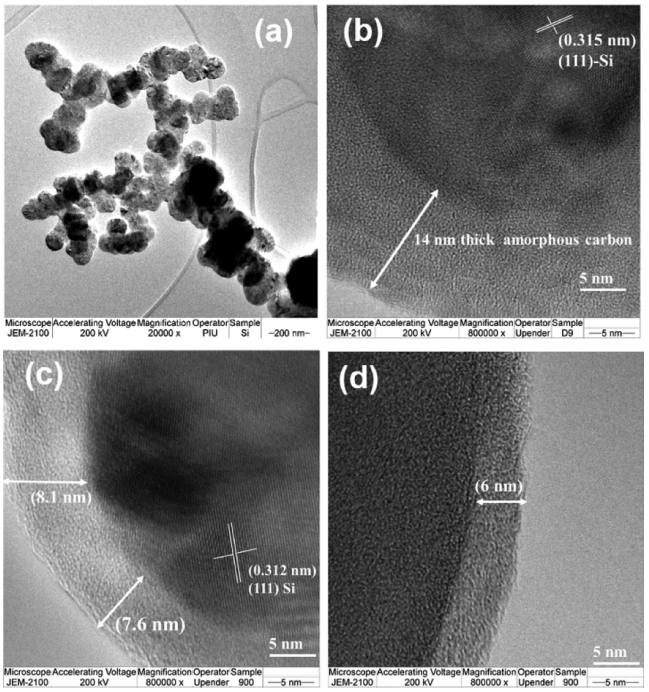

Figure 3. TEM images of (a) Si NPs synthesized by magnesiothermic reduction; Si−C composite annealed at (b) 700, (c) 900, and (d) 1000 °C indicating carbon coating, lattice fringes, and atomic layers (scale bar: 5 nm).

enough space for free expansion and contraction of silicon during alloying and dealloying with lithium. Si−C composite annealed between 700 and 1000 °C (Figure 2d,e) shows a partial increase in particle size of Si-NPs because of the coalescence or nucleation of particles leading to agglomeration compared to pristine silicon (Figure 2a).

The Brunauer−Emmett−Teller (BET) surface area of Si−C composites were found to be 105, 46, and 15.8 m^2 g^{-1} annealed at 700, 900, and 1000 °C. As expected, SEM and transmission electron microscopy (TEM) images of pure Si-NPs converge. Si-NPs have 50−100 nm in size (Figure 3a). Si−C composite electrodes annealed between 700 and 1000 °C show Si-NP particles covered by a thick carbon film about 14 nm. The crystallites have a typical, well-defined face-centered cubic symmetry, and the atomic layers are also clearly observed. The *d*-spacing values of about 0.315 nm correspond to 111 reflections in the XRD pattern of Si. Si−C composite electrodes annealed between 900 and 1000 °C show about 8 and 6 nm of thick carbon coatings, respectively, onto Si-NPs. The thickness of carbon coating decreases with increase of temperature. At a high temperature of 1000 °C, the carbon coating becomes more compact because of which carbon layer binds strongly to silicon NPs and carbon fibers because of which the thickness of carbon coating decreases. This implies that with increasing temperature, the carbon coatings sinter, allowing to gain more mechanical strength. This increase in mechanical strength helps in increasing the physical binding of carbon, silicon, and CFs. The carbon coatings are stronger and compact on increasing the temperature, allowing the silicon volume change during cycling without undergoing pulverization.

Raman spectra (Figure 4) of silicon−carbon composite fabricated at different temperatures correspond to Si−Si stretching (peak at 512 cm^{-1}), and D-band (disorder band)

DOI: 10.1021/acsomega.8b00924
ACS Omega 2018, 3, 9598−9606

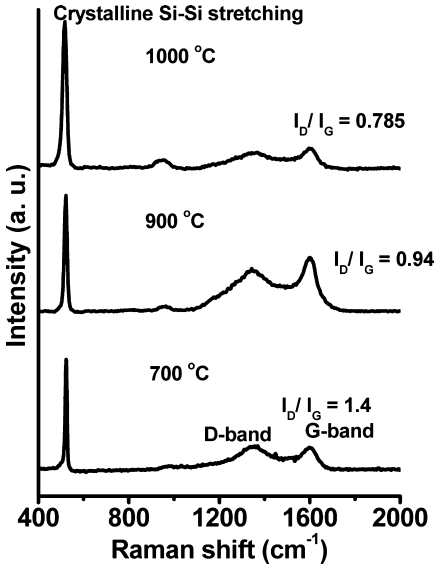

Figure 4. Raman spectrum of silicon−carbon composite formed by calcination at different temperatures 700, 900, and 1000 °C for 5 h under argon atmosphere.

and G-band (graphitic band) at 1355 and 1597 cm^{-1}, respectively. The presence of silicon and carbon peaks indicates the successful formation of Si−C composite. The integral intensity ratio of D to G bands for the Si−C composite samples annealed at 700−1000 °C was estimated to be 1.4 and 0.785, which indicates the formation of disordered carbons. The decrease of D/G ratio with an increase of temperature in Figure 4 suggests the increase in graphitic nature with increase of temperature. This, in turn, increases the conductivity of the electrode material.

Reversible capacity and cycle stability of silicon anodes significantly reduce upon cycling at deep cutoff potentials. Cycling silicon anodes above 50 mV reduce the formation of crystalline phases and result in good electrochemical performance.[46,47] Thus, galvanostatic charge−discharge cycling of our Si-NPs was carried out in the potential range between 1.2 and 0.05 V. The 3D Si−C composite electrodes annealed at different temperatures show higher reversible capacity (Figure 5a) compared to conventional silicon composite electrode which suggest 3D electrode architecture and enables the complete utilization of active material coated onto the CF compared to conventional silicon electrode. The conventional silicon composite electrodes show a high irreversible capacity of 48% with an initial lithiation capacity of 3201 mA h g^{-1}. High irreversible capacity is attributed to the high intake of Li during the formation of SEI in the conventional Si composite electrode. The low conductivity of the composite electrode and pulverization lead to rapid capacity fade of Si-NPs in conventional composite electrode.

The initial lithiation capacity of 3D Si−C free-standing composite electrodes annealed at 1000, 900, and 700 °C were 2193, 2712, and 3533 mA h g^{-1} and that for conventional electrode was 3201 mA h g^{-1} at 0.1 C rate, and the corresponding irreversible capacities were 11, 16, 18, and 48% during 1st cycle. The improvement in irreversible capacity of 3D Si−C free-standing composite electrodes during first cycle is due to the coating of carbon onto silicon NPs which reduces the side reactions of silicon with electrolyte; this in turn reduces with an increase in the annealing temperature

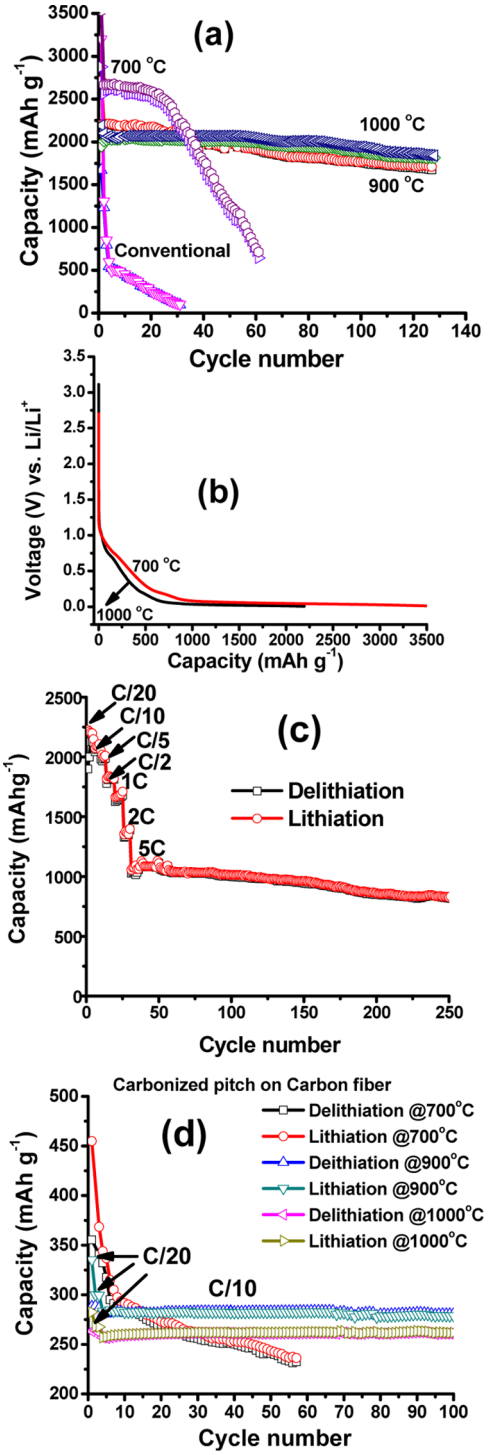

Figure 5. (a) Comparison of cycle life of 3D Si−C composite electrodes prepared at 700, 900, 1000 °C, and conventional electrode (as indicated), (b) voltage profiles during lithiation process for the freestanding electrode annealed at 700 and 1000 °C, (c) C-rate performance for the Si−C composite free-standing electrode annealed at 1000 °C, and (d) capacity vs cycle number for the pitch-coated CFs (no Si-NPs) annealed at 700, 900, and 1000 °C (as indicated).

(Figure 5b). Si−C composite annealed at 700 °C shows an initial high discharge capacity than that of the Si−C composite electrodes annealed at 900 and 1000 °C; this is due to the high surface area of Si−C composite annealed at 700 °C than that at 900 and 1000 °C. In discharge voltage profile, there is a plateau

DOI: 10.1021/acsomega.8b00924
ACS Omega 2018, 3, 9598−9606

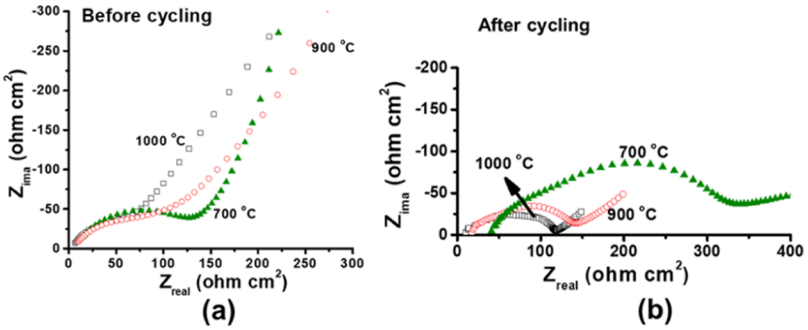

Figure 6. Nyquist plots for the Si-NPs for the 3D CF electrodes annealed at 700−1000 °C (as indicated) in the frequency range between 1 MHz and 10 mHz during (a) before cycling at OCV and (b) after 60 cycles delithiation for 700 °C and after 100 cycles for 900 and 1000 °C.

below 1 V (Figure 4b and Supporting Information Figure S3) which is due to the alloying of Li^+ with silicon and the plateau from 0.25 to 0.5 V during charging (Supporting Information Figure S3) and dealloying of Li^+ with silicon. All of the 3D Si−C free-standing electrodes annealed between 700 and 1000 °C show similar voltage profiles (Figure 5b and Supporting Information Figure S3). The 3D Si−C free-standing composite electrode shows an enhanced electrochemical performance than that of the conventional silicon electrode. In this architecture, coating of carbonized pitch onto silicon NPs efficiently prevents the direct exposure of Si-NPs to electrolyte which helps in maintaining the interfacial and structural stability. In addition to this, the 3D CF and carbonized pitch effectively accommodate the volume expansion and contraction, thus enabling the electrical and structural integrity of the electrode. Figure 5a shows that the 3D Si−C electrodes at 700 °C show a high initial stable discharge capacity (∼2600 mA h g^{-1}) than that at 900 °C (2220 mA h g^{-1}) and 1000 °C (2060 mA h g^{-1}) which is due to the high surface area (105 m^2 g^{-1}) of Si−C composite. However, the Si−C composite annealed at 700 °C shows a rapid capacity fade with a progress of cycling (after 25 cycles), whereas Si−C composite electrodes annealed at 900 and 1000 °C show enhanced electrochemical performance in terms of capacity retention and cyclability (Figure 5a). The 3D Si−C composite electrodes annealed at 1000 °C show very stable capacity of about 2000 mA h g^{-1} for over 130 cycles with little loss in capacity (∼5%), whereas about 25% capacity loss was observed for the electrodes annealed at 900 °C. High capacity retention is because of the high conductivity of 3D Si−C composite electrodes annealed at 1000 °C compared to 900 °C. The C-rate performance of Si−C free-standing electrodes annealed at 1000 °C shows ∼1000 mA h g^{-1} capacity at 5 C rate which could be achieved, and these cells cycle very well for over 250 cycles with little loss in capacity. We have further evaluated the capacity contribution from the carbon derived from pitch and CFs used in this study. The pitch-coated carbons on CF annealed at 900 and 1000 °C show very stable capacities between 250 and 280 mA h g^{-1} (Figure 5d). The pitch-coated carbons on CF annealed at 700 °C with a high initial capacity of >300 mA h g^{-1}, and the capacity reduces to 225 mA h g^{-1} in 60 cycles.

The electrochemical impedance spectroscopy (EIS) behavior of Si−carbon composite 3D electrode architectures annealed between 700 and 1000 °C before and after cycling have been investigated to further understand the kinetics of electrochemical processes which influence the electrochemical performance. The impedance spectra of Si−C composite 3D electrodes were measured in equilibrium conditions using lithium reference electrode, as shown in Figure 6. The impedance of 3D Si−C composite electrode annealed at 1000 °C has a low Ohmic (2.07 Ω cm^2) and charge-transfer resistance (151.45 Ω cm^2) before cycling and that of the electrode fabricated at 700 °C shows 10.14 Ω cm^2 and 183.46 Ω cm^2 (Figure 6a). The electrode fabricated at 900 °C shows intermediate resistances (6.50 and 156.67 Ω cm^2) (Figure 6a). The Ohmic resistance of the electrode fabricated at 900 °C increases to 17.14 Ω cm^2 and a charge-transfer resistance increases to 158.57 Ω cm^2 after 100 cycles, whereas the electrode fabricated at 700 °C shows high an Ohmic resistance of 39.96 Ω cm^2 and a charge-transfer resistance of 366.18 Ω cm^2 after 60 cycles (Figure 6b). The impedance analysis shows the contribution of both surface resistance and solid-state diffusion through the bulk of the Si-NPs. The surface process is dominated by an SEI layer consisting of an inner, inorganic insoluble part and several organic compounds at the outer interface. The surface resistivity, which seems to be correlated with the coulombic efficiency of the electrode, grows at very high lithium contents because of an increase in the inorganic SEI thickness. EIS illustrates that on increasing the annealing temperature, there is an improvement in conductivity which in turn helps in improving the electrochemical performance.

Postmortem analyses of active materials after 60 cycles for Si-NPs annealed at 700 °C and after 100 cycles for Si-NPs annealed at 900 and 1000 °C are shown in Supporting Information Figure S4a−c; respectively. From SEM images of Figure S4a, it is observed that the electrode annealed at 700 °C shows the cracks and complete degradation of the material leading to the failure of electrochemical performance, whereas the electrode annealed at 900 °C presented in Figure S4b shows a dispersed carbon-coated silicon NPs and less cracks and less degradation compared to 3D-Si−C annealed at 700 °C. Si−C electrodes annealed at 1000 °C (Figure S4c) show particles similar to pristine particles, as shown in Figure 2f with very less change in morphology even after cycling compared to other temperature 3D electrodes. From the above observation, it is clear that the mechanical strength of Si-NPs increases with increase of temperature and maintains the integrity of the particles during cycling which attributes to the improved electrochemical performance.

To characterize the performance of Si−carbon composite 3D electrode as an anode, the electrochemical performance of Si−C-composite anode and Mg−F-doped LMR−NMC ($Li_{1.2}Ni_{0.13}Mn_{0.55}Co_{0.1}Mg_{0.02}O_{2-x}F_x$) composite cathodes was tested in a full-cell configuration.[48] The Mg−F-doped LMR−NMC cathodes deliver as high as 300 mA h g^{-1} capacity (Supporting Information Figure S5) and cycles very well.[48]

DOI: 10.1021/acsomega.8b00924
ACS Omega 2018, 3, 9598−9606

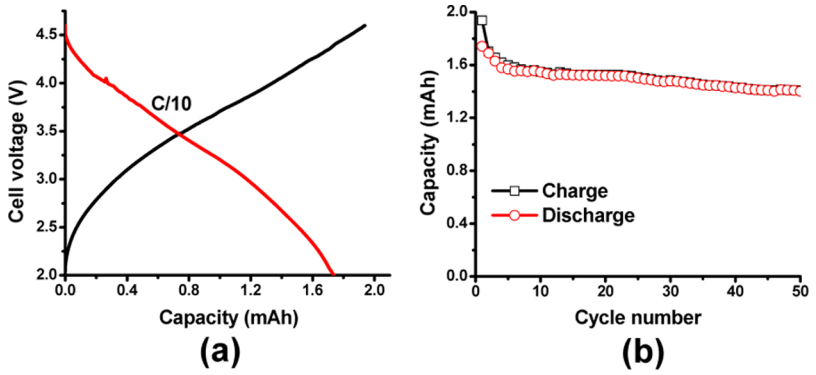

Figure 7. (a) Charge−discharge voltage profile, (b) cycle life data of full cell consisting of Si−carbon 3D composite electrode as an anode with Mg−F-doped LMR−NMC cathode at C/10 rate.

Coin cells fabricated using Si−carbon composite 3D electrode and Mg−F-doped LMR−NMC cathode shows a high open-circuit voltage of >4 V (Figure 7) and a high energy density of >500 W h kg^{-1} (calculated from the integration of discharge capacity) in the voltage range between 4.6 and 2.0 V, as shown in Figure 7. The irreversible capacity for these cells was less than 10%. These coin cells show stable cycling for 50 cycles with little loss in capacity. Further improvements in electrochemical performance in full cells in pouch-type configuration are underway.

3. DISCUSSIONS

The 3D electrode architecture of Si-NPs on CF allows the continuous conducting framework having excellent electronic properties, adaptable and flexible medium (carbon formed from the pitch and CF) which accommodates the volume change of silicon during lithiation and delithiation. Further, increasing the temperature from 700 to 1000 °C increases the structural ordering of carbon and silicon, which allows coating of carbon layers throughout Si-NPs. The carbon coating increases the contact strength of carbon with silicon and CF, thereby increasing the mechanical strength of 3D-Si−C composite electrode. The integrity of the Si−C composite material is well-maintained largely because of the mechanical strength of the CF and pitch. When the electrodes are fabricated with CFs coated with pitch and Si-NPs, the pitch improves the connectivity between fiber−fiber and fiber−Si active material contacts, thereby reducing the total internal impedance of the cell. During lithiation and delithiation, carbon strongly holds silicon and allows expansion and contraction without undergoing pulverization. In addition, the improvement in conductivity with an increase of temperature also enhances the electrochemical performance. The 3D electrode CF architecture with pitch controls the degradation of the Si anode. All of these features offer ample opportunities for modifying toward better Si-anode materials for an optimal cell performance.

4. CONCLUSIONS

Organic binder and conducting diluent-free 3D silicon−carbon free-standing electrodes prepared at 1000 °C shows excellent electrochemical performance. Reversible capacities over 2000 mA h g^{-1} at C/10 rate and ∼1000 mA h g^{-1} at 5 C rate could be obtained for these electrodes for 250 charge−discharge cycles. Pitch provides a very thin layer of coating between 6 and 14 nm (annealed at temperature between 700 and 1000 °C) onto Si-NPs and improves the connectivity between fiber−fiber and fiber−Si active-material contacts, thereby reducing the total internal impedance of the cell. During insertion and extraction of Li, carbon strongly holds Si NPs and allows the expansion and contraction without undergoing pulverization. The 3D CF electrode architecture with pitch controls the degradation of Si anode and improves the overall electrochemical performance during cycling. Besides, usual copper foil current collector is replaced by CFs which in fact contributes about 10% capacity of Si−C composite electrodes. Besides, carbonized pitch delivers a capacity (260−280 mA h g^{-1}) to the total capacity of the electrode. The Si−C composite electrodes do not contain any organic binder such as PVdF, which does not contribute to the capacity. All of these factors contribute toward improved energy density of Si−C composite electrodes. Unlike other expensive methods used for the fabrication of free-standing electrodes, the electrode fabrication process presented here is inexpensive and scalable. Full cells fabricated using Si−carbon composite electrode and Mg−F-doped LMR−NMC cathode shows a high open-circuit voltage of >4 V and a high energy density of >500 W h kg^{-1} in the voltage range between 4.6 and 2.0 V.

5. EXPERIMENTAL SECTION

5.1. Synthesis and Structural and Morphological Characterizations. Silicon NPs are synthesized by magnesiothermic reduction of fumed silica.[15,47] In brief, 1:2 mol ratio of fumed silica and magnesium powder are mixed thoroughly in a mortar pestle for 1 h, followed by annealing at 700 °C under argon gas for 2 h. The obtained product was treated with 1 N HCl solution to eliminate MgO and Mg_2Si-producing pure Si-NPs. Powder XRD patterns of Si-NPs, CFs, and so forth were performed by using a PANalytical X'Pert Pro diffractometer (The Netherlands) [reflection $\theta-\theta$ geometry, Cu Kα (1.54 Å) radiation]. The diffraction data were collected at 0.02 step widths over a 2θ range from 20 to 60°. The surface morphologies of the composite powders were measured by a scanning electron microscope (Carle Zeiss SUPRA 40, field emission scanning electron microscope) coupled with Thermo NORAN EDS system for surface element analysis, TEM (JEOL-JSM-700F), and the physical properties by Raman spectroscopy using a micro-Raman spectrometer HR800 (Jobin Yovn Horiba, France), with He−Ne laser (excitation line 632.8 nm) and a microscope objective (50×, Olympus Mplan, 0.4 mm working, numerical aperture 0.75 in back-scattering configuration). The surface area of the Si−C

DOI: 10.1021/acsomega.8b00924
ACS Omega 2018, 3, 9598−9606

composites annealed at 700, 900, and 1000 °C are measured by BET experiment (Quantachrome instruments, USA). Mg- and F-doped (0.02 mol % of Mg and 1:50 wt %—LiF:LMR–NMC) LMR–NMC material was synthesized, as described in our earlier report.[48]

Mg- and F-doped LMR–NMC composite cathodes are chosen as they deliver stable energy over cycles compared to pristine LMR–NMC.[48] LMR–NMC composite cathodes have significant energy loss during cycling.[6,48]

5.2. 3D Electrode Fabrication. CF mats having diameter in the range between 5 and 10 μm (Supporting Information Figure S1a) are obtained from advanced fiber nonwovens (Hollingsworth & Vose Company, MA, USA) and are mostly nongraphitic in nature (only disordered carbons) (Supporting Information Figure S1b). Graphitic CFs are not used as they are very brittle. The current CFs have a good mechanical strength, flexibility and electrical conductivity on the order of 10^4 S cm^{-1}. A 1:1 wt ratio of Si-NPs and P-pitch isthoroughly mixed with the required amount of *N*-vinyl pyrrolidone to make slurry followed by coating on CF mats. The coated mats are dried at 90 °C under vacuum overnight followed by punching, calendaring, and carbonizing the electrodes at 700–900–1000 °C for 5 h under argon atmosphere (hereafter, the electrodes are called Si–C composite electrodes on 3D CF). At a temperature of ≥700 °C, P-pitch forms a foamlike structure (Supporting Information Figure S1c) and coats on to Si-NPs and along CFs. Thereby, P-pitch makes a good electronic contact between Si-NPs and CFs. The electrode structure of 700 °C annealed sample is shown in Supporting Information Figure S1d. The complete scheme of electrode fabrication is presented in Supporting Information Figure S2. The loading of Si–C composite on CF was between 6 and 10 mg cm^{-2}, which is much higher than the reported value.[35]

5.3. Electrochemical Performance Studies. The electrochemical performance of the samples comprising pristine silicon NPs, on copper foil (conventional electrode) and only pitch-coated CF, and finally silicon–carbon composite on CF as active masses were measured by using Solartron cell test system consisting 1470E multichannel potentiostats and multiple 1455A series frequency response analyzers (driven by Corrware and ZPlot software from Scribner Associates) and Arbin battery cycler (Arbin BT2000—battery test equipment, USA). The impedance measurements were carried out in a frequency range between 1 MHz and 10 mHz before cycling on an open-circuit condition (OCV) and in full charged condition after 100 cycles. The conventional electrodes were prepared by making the composite of 60% active material, 10% PVdF (Kynar), and 30% carbon black (Super C65, Timcal; Nanoshell, USA) in *N*-methyl pyrrolidone (Sigma-Aldrich) coated on to the copper foil (>99.9%, Strem chemicals, Inc., USA) current collector by using the doctor blade technique. All of the composite electrodes were dried under vacuum at 90 °C, followed by punching them into 1 cm^2 area circular discs. The cells were fabricated in a glovebox (M-Braun, Germany) filled with ultrahigh purity argon (99.999%). The moisture and oxygen content of the glovebox was less than 0.1 ppm. CR2032 coin-type cells (MTI, China) were assembled using lithium foil as a counter electrode, polyethylene–polypropylene trilayer (Celgard Inc.) as a separator, and conventional silicon electrode or silicon–carbon composite on CF or only CF as working electrodes, and 1 M $LiPF_6$ in 1:1 ratio of ethylene carbonate and dimethyl carbonate as the electrolyte. Charge–discharge cycling was carried out in the potential range between 1.2 V and 50 mV using constant current. Full cells are assembled with Mg–F-doped LMR–NMC composite cathodes and current silicon anodes (developed at IIT Hyderabad) and cycled in the potential range between 2.0 and 4.65 V.[48] All electrochemical tests are a conducted set of at least four cells at each temperatures and are reproducible.

■ ASSOCIATED CONTENT

Supporting Information

The Supporting Information is available free of charge on the ACS Publications website at DOI: 10.1021/acsomega.8b00924.

Structure and morphology of CF, SEM image of carbonized pitch, and Si–C electrode; schematics of electrode fabrication process; capacity versus voltage profile plots; and SEM images of cycled Si–C active materials annealed at 700, 900, and 1000 °C (PDF)

■ AUTHOR INFORMATION

Corresponding Author

*E-mail: martha@iith.ac.in (Surendra K. Martha).

ORCID

Jagjit Nanda: 0000-0002-6875-0057

Surendra K. Martha: 0000-0002-7762-7237

Notes

The authors declare no competing financial interest.

■ ACKNOWLEDGMENTS

S.K.M. acknowledges DST-SERB (grant no. SB/FT/CS-147/2014) for the financial support. We thank the TEM facility and Upender Sunkari, IIT Hyderabad, India, for the microscopy support. Work at Oak Ridge National Laboratory is supported by the Assistant Secretary for Energy Efficiency and Renewable Energy, Office of Vehicle Technologies of the U.S. Department of Energy under Contract No. DE-AC02-05CH11231.

■ REFERENCES

(1) USABC Goals for Advanced Batteries for EVs—CY 2020 Commercialization, http://www.uscar.org/guest/article_view.php?articles_id=85, USABC, 2017.

(2) Choi, J. W.; Aurbach, D. Promise and reality of post-lithium-ion batteries with high energy densities. *Nat. Rev. Mater.* **2016**, *1*, 16013.

(3) Thackeray, M. M.; Kang, S.-H.; Johnson, C. S.; Vaughey, J. T.; Benedek, R.; Hackney, S. A. Li_2MnO_3-stabilized $LiMO_2$ (M = Mn, Ni, Co) electrodes for lithium-ion batteries. *J. Mater. Chem.* **2007**, *17*, 3112.

(4) Nayak, P. K.; Erickson, E. M.; Schipper, F.; Penki, T. R.; Munichandraiah, N.; Adelhelm, P.; Sclar, H.; Amalraj, F.; Markovsky, B.; Aurbach, D. Review on Challenges and Recent Advances in the Electrochemical Performance of High Capacity Li- and Mn-Rich Cathode Materials for Li-Ion Batteries. *Adv. Energy Mater.* **2017**, *8*, 1702397.

(5) Zheng, J.; Myeong, S.; Cho, W.; Yan, P.; Xiao, J.; Wang, C.; Cho, J.; Zhang, J.-G. Li- and Mn-Rich Cathode Materials: Challenges to Commercialization. *Adv. Energy Mater.* **2017**, *7*, 1601284.

(6) Martha, S. K.; Nanda, J.; Veith, G. M.; Dudney, N. J. Electrochemical and rate performance study of high-voltage lithium-rich composition: $Li_{1.2}Mn_{0.525}Ni_{0.175}Co_{0.1O2}$. *J. Power Sources* **2012**, *199*, 220–226.

(7) Su, X.; Wu, Q.; Li, J.; Xiao, X.; Lott, A.; Lu, W.; Sheldon, B. W.; Wu, J. Silicon-Based Nanomaterials for Lithium-Ion Batteries: A Review. *Adv. Energy Mater.* **2014**, *4*, 1300882.

DOI: 10.1021/acsomega.8b00924
ACS Omega 2018, 3, 9598–9606

(8) Zhang, W.-J. A review of the electrochemical performance of alloy anodes for lithium-ion batteries. *J. Power Sources* **2011**, *196*, 13−24.
(9) Chan, C. K.; Peng, H.; Liu, G.; McIlwrath, K.; Zhang, X. F.; Huggins, R. A.; Cui, Y. High-performance lithium battery anodes using silicon nanowires. *Nat. Nanotechnol.* **2008**, *3*, 31−35.
(10) Gu, M.; He, Y.; Zheng, J.; Wang, C. Nanoscale silicon as anode for Li-ion batteries: The fundamentals, promises, and challenges. *Nano Energy* **2015**, *17*, 366−383.
(11) Obrovac, M. N.; Christensen, L. Structural Changes in Silicon Anodes during Lithium Insertion/Extraction. *Electrochem. Solid-State Lett.* **2004**, *7*, A93−A96.
(12) Ryu, J. H.; Kim, J. W.; Sung, Y.-E.; Oh, S. M. Failure Modes of Silicon Powder Negative Electrode in Lithium Secondary Batteries. *Electrochem. Solid-State Lett.* **2004**, *7*, A306−A309.
(13) Jaumann, T.; Herklotz, M.; Klose, M.; Pinkert, K.; Oswald, S.; Eckert, J.; Giebeler, L. Tailoring Hollow Silicon-Carbon Nanocomposites As High-Performance Anodes in Secondary Lithium-Based Batteries through Economical Chemistry. *Chem. Mater.* **2015**, *27*, 37−43.
(14) Kim, H.; Han, B.; Choo, J.; Cho, J. Three-Dimensional Porous Silicon Particles for Use in High-Performance Lithium Secondary Batteries. *Angew. Chem., Int. Ed.* **2008**, *120*, 10305−10308.
(15) Gao, P.; Tang, H.; Xing, A.; Bao, Z. Porous silicon from the magnesiothermic reaction as a high-performance anode material for lithium ion battery applications. *Electrochim. Acta* **2017**, *228*, 545−552.
(16) Wang, W.; Kumta, P. N. Nanostructured Hybrid Silicon/Carbon Nanotube Heterostructures: Reversible High-Capacity Lithium-Ion Anodes. *ACS Nano* **2010**, *4*, 2233−2241.
(17) Qu, J.; Li, H.; Henry, J. J., Jr.; Martha, S. K.; Dudney, N. J.; Xu, H.; Chi, M.; Lance, M. J.; Mahurin, S. M.; Besmann, T. M.; Dai, S. Self-aligned Cu-Si core-shell nanowire array as a high-performance anode for Li-ion batteries. *J. Power Sources* **2012**, *198*, 312−317.
(18) Song, H.; Wang, H. X.; Lin, Z.; Jiang, X.; Yu, L.; Xu, J.; Yu, Z.; Zhang, X.; Liu, Y.; He, P.; Pan, Y.; Shi, Y.; Zhou, H.; Chen, K. Highly Connected Silicon-Copper Alloy Mixture Nanotubes as High-Rate and Durable Anode Materials for Lithium-Ion Batteries. *Adv. Funct. Mater.* **2016**, *26*, 524−531.
(19) Toan, L. T.; Moyen, E.; Zamfir, M. R.; Joe, J.; Kim, Y. W.; Pribat, D. Si nanowires grown by Al-catalyzed plasma-enhanced chemical vapor deposition: synthesis conditions, electrical properties and application to lithium battery anodes. *Mater. Res. Express* **2016**, *3*, 015003.
(20) Chen, Y.; Hu, Y.; Shen, Z.; Chen, R.; He, X.; Zhang, X.; Li, Y.; Wu, K. Hollow core-shell structured silicon@carbon nanoparticles embed in carbon nanofibers as binder-free anodes for lithium-ion batteries. *J. Power Sources* **2017**, *342*, 467−475.
(21) Qin, J.; Wu, M.; Feng, T.; Chen, C.; Tu, C.; Li, X.; Duan, C.; Xia, D.; Wang, D. High rate capability and long cycling life of graphene-coated silicon composite anodes for lithium ion batteries. *Electrochim. Acta* **2017**, *256*, 259−266.
(22) Tang, J.; Dysart, A. D.; Kim, D. H.; Saraswat, R.; Shaver, G. M.; Pol, V. G. Fabrication of Carbon/Silicon Composite as Lithium-ion Anode with Enhanced Cycling Stability. *Electrochim. Acta* **2017**, *247*, 626−633.
(23) Kim, H.; Cho, J. Superior Lithium Electroactive Mesoporous Si@Carbon Core−Shell Nanowires for Lithium Battery Anode Material. *Nano Lett.* **2008**, *8*, 3688−3691.
(24) Bai, X.; Yu, Y.; Kung, H. H.; Wang, B.; Jiang, J. Si@SiO x /graphene hydrogel composite anode for lithium-ion battery. *J. Power Sources* **2016**, *306*, 42−48.
(25) Morita, T.; Takami, N. Nano Si Cluster-SiO_x−C Composite Material as High-Capacity Anode Material for Rechargeable Lithium Batteries. *J. Electrochem. Soc.* **2006**, *153*, A425−A430.
(26) Roy, A. K.; Zhong, M.; Schwab, M. G.; Binder, A.; Venkataraman, S. S.; Tomović, Z. Preparation of a Binder-Free Three-Dimensional Carbon Foam/Silicon Composite as Potential Material for Lithium Ion Battery Anodes. *ACS Appl. Mater. Interfaces* **2016**, *8*, 7343−7348.
(27) Fei, L.; Williams, B. P.; Yoo, S. H.; Kim, J.; Shoorideh, G.; Joo, Y. L. Graphene Folding in Si Rich Carbon Nanofibers for Highly Stable, High Capacity Li-Ion Battery Anodes. *ACS Appl. Mater. Interfaces* **2016**, *8*, 5243−5250.
(28) Xie, J.; Tong, L.; Su, L.; Xu, Y.; Wang, L.; Wang, Y. Core-shell yolk-shell Si@C@Void@C nanohybrids as advanced lithium ion battery anodes with good electronic conductivity and corrosion resistance. *J. Power Sources* **2017**, *342*, 529−536.
(29) David, L.; Bhandavat, R.; Barrera, U.; Singh, G. Silicon oxycarbide glass-graphene composite paper electrode for long-cycle lithium-ion batteries. *Nat. Commun.* **2016**, *7*, 10998.
(30) Maranchi, J. P.; Hepp, A. F.; Kumta, P. N. High Capacity, Reversible Silicon Thin-Film Anodes for Lithium-Ion Batteries. *Electrochem. Solid-State Lett.* **2003**, *6*, A198−A201.
(31) Shoorideh, G.; Ko, B.; Berry, A.; Divvela, M. J.; Kim, Y. S.; Li, Z.; Patel, B.; Chakrapani, S.; Joo, Y. L. Harvesting Interconductivity and Intraconductivity of Graphene Nanoribbons for a Directly Deposited, High-Rate Silicon-Based Anode for Li-Ion Batteries. *ACS Appl. Energy Mater.* **2018**, *1*, 1106−1115.
(32) Suresh, S.; Wu, Z. P.; Bartolucci, S. F.; Basu, S.; Mukherjee, R.; Gupta, T.; Hundekar, P.; Shi, Y.; Lu, T.-M.; Koratkar, N. Protecting Silicon Film Anodes in Lithium-Ion Batteries Using an Atomically Thin Graphene Drape. *ACS Nano* **2017**, *11*, 5051−5061.
(33) Polat, D. B.; Keles, O.; Amine, K. Compositionally-graded silicon-copper helical arrays as anodes for lithium-ion batteries. *J. Power Sources* **2016**, *304*, 273−281.
(34) Maranchi, J. P.; Hepp, A. F.; Kumta, P. N. High Capacity, Reversible Silicon Thin-Film Anodes for Lithium-Ion Batteries. *Electrochem. Solid-State Lett.* **2003**, *6*, A198−A201.
(35) Murugesan, S.; Harris, J. T.; Korgel, B. A.; Stevenson, K. J. Copper-Coated Amorphous Silicon Particles as an Anode Material for Lithium-Ion Batteries. *Chem. Mater.* **2012**, *24*, 1306−1315.
(36) Lee, J. K.; Smith, K. B.; Hayner, C. M.; Kung, H. H. Silicon nanoparticles-graphene paper composites for Li ion battery anodes. *Chem. Commun.* **2010**, *46*, 2025−2027.
(37) Thakur, M.; Pernites, R. B.; Nitta, N.; Isaacson, M.; Sinsabaugh, S. L.; Wong, M. S.; Biswal, S. L. Freestanding Macroporous Silicon and Pyrolyzed Polyacrylonitrile As a Composite Anode for Lithium Ion Batteries. *Chem. Mater.* **2012**, *24*, 2998−3003.
(38) Cui, L.-F.; Hu, L.; Choi, J. W.; Cui, Y. Light-Weight Free-Standing Carbon Nanotube-Silicon Films for Anodes of Lithium Ion Batteries. *ACS Nano* **2010**, *4*, 3671−3678.
(39) Gowda, S. R.; Pushparaj, V.; Herle, S.; Girishkumar, G.; Gordon, J. G.; Gullapalli, H.; Zhan, X.; Ajayan, P. M.; Reddy, A. L. M. Three-Dimensionally Engineered Porous Silicon Electrodes for Li Ion Batteries. *Nano Lett.* **2012**, *12*, 6060−6065.
(40) Wang, X.; Li, G.; Seo, M. H.; Lui, G.; Hassan, F. M.; Feng, K.; Xiao, X.; Chen, Z. Carbon-Coated Silicon Nanowires on Carbon Fabric as Self-Supported Electrodes for Flexible Lithium-Ion Batteries. *ACS Appl. Mater. Interfaces* **2017**, *9*, 9551−9558.
(41) Yehezkel, S.; Auinat, M.; Sezin, N.; Starosvetsky, D.; Ein-Eli, Y. Bundled and densified carbon nanotubes (CNT) fabrics as flexible ultra-light weight Li-ion battery anode current collectors. *J. Power Sources* **2016**, *312*, 109−115.
(42) Martha, S. K.; Nanda, J.; Zhou, H.; Idrobo, J. C.; Dudney, N. J.; Pannala, S.; Dai, S.; Wang, J.; Braun, P. V. Electrode architectures for high capacity multivalent conversion compounds: iron (II and III) fluoride. *RSC Adv.* **2014**, *4*, 6730−6737.
(43) Martha, S. K.; Kiggans, J. O.; Nanda, J.; Dudney, N. J. Advanced Lithium Battery Cathodes Using Dispersed Carbon Fibers as the Current Collector. *J. Electrochem. Soc.* **2011**, *158*, A1060−A1066.
(44) Klett, J.; Hardy, R.; Romine, E.; Walls, C.; Burchell, T. High-thermal-conductivity, mesophase-pitch-derived carbon foams: effect of precursor on structure and properties. *Carbon* **2000**, *38*, 953−973.

DOI: 10.1021/acsomega.8b00924
ACS Omega 2018, 3, 9598−9606

(45) Andrews, R.; Jacques, D.; Qian, D.; Dickey, E. C. Purification and structural annealing of multiwalled carbon nanotubes at graphitization temperatures. *Carbon* **2001**, *39*, 1681−1687.
(46) Beattie, S. D.; Loveridge, M. J.; Lain, M. J.; Ferrari, S.; Polzin, B. J.; Bhagat, R.; Dashwood, R. Understanding capacity fade in silicon based electrodes for lithium-ion batteries using three electrode cells and upper cut-off voltage studies. *J. Power Sources* **2016**, *302*, 426−430.
(47) Sarode, K. K.; Choudhury, R.; Martha, S. K. Binder and conductive additive free silicon electrode architectures for advanced lithium-ion batteries. *J. Energy Storage* **2018**, *17*, 417−422.
(48) Kumar, S. K.; Ghosh, S.; Martha, S. K. Synergistic effect of magnesium and fluorine doping on the electrochemical performance of lithium-manganese rich (LMR)-based Ni-Mn-Co-oxide (NMC) cathodes for lithium-ion batteries. *Ionics* **2017**, *23*, 1655−1662.

DOI: 10.1021/acsomega.8b00924
ACS Omega 2018, 3, 9598−9606